J Mater Sci (2011) 46:648–658
DOI 10.1007/s10853-010-4787-7

Preparation of isotactic polypropylene-grafted multiwalled carbon nanotubes (iPP-g-MWNTs) by macroradical addition in solution and the properties of iPP-g-MWNTs/iPP composites

Jun Zheng · Zhongming Zhu · Ji Qi · Zhi Zhou · Peng Li · Mao Peng

Received: 12 January 2010 / Accepted: 22 July 2010 / Published online: 7 August 2010

Abstract Isotactic polypropylene (iPP) was successfully grafted onto multiwalled carbon nanotubes (MWNTs) by direct macroradical addition by sonication in hot xylene with BPO as an initiator. A quantitative determination of the grafting ratio was first realized after the iPP-g-MWNTs were extensively purified by repeated hot vacuum filtration and redispersion in xylene at 130 °C. It was found that both iPP macromolecular radicals and small-molecular benzoic acid free radicals were grafted onto MWNTs. iPP-g-MWNTs dispersed more uniformly in iPP than pristine MWNTs. The iPP-g-MWNTs/iPP composites have much higher elongations at break than the iPP composites filled with pristine MWNTs, and the Young's modulus and yield strength were also improved to some extent. iPP-g-MWNTs also have a stronger nucleation effect on the crystallization of iPP than pristine MWNTs.

Introduction

Carbon nanofibers and carbon nanotubes (CNTs), including multiwalled carbon nanotubes (MWNTs) and single-walled carbon nanotubes (SWNTs), are attractive nanofillers for polymer composites because of the improved mechanical, electrical and thermal conductivities, heat resistance, and reduced flammability, etc. [1–8] Since 1990s, nanofillers/polymer composites have been actively investigated, in which, effective surface modification and uniform dispersion of CNTs in the polymer matrices are the focus of research interests because of their crucial roles for preparing high performance composites.

Chemical modifications are widely accepted to be effective to immobilize functional groups on CNTs and improve the affinity between CNTs and the polymer matrices. Among the chemical modification reactions of CNTs, free radical addition reaction has been demonstrated to be relatively facile and energy efficient to functionalize CNTs covalently [9–14]. Both small-molecular free radicals and macroradicals can be coupled with CNTs. For example, in situ radical polymerization of various vinyl monomers on CNTs could result in the formation of polymer-grafted CNTs [15–17]. Bromide-ended polystyrene (PS) was used to produce PS radicals and synthesize PS-grafted CNTs in the presence of ATRP co-initiators [18]. TEMPO group capped poly(2-vinypyridine) [19], nitroxide-terminated PS [15], and azide-functionalized polymer [16] were used to generate macroradicals and terminate onto the surface of CNTs. Chain cleavage of weak bonds on macromolecules was used to generate macroradicals, e.g., azo-group carrying macroinitiator was been synthesized for the modification of SWNTs [11]. Moreover, common polymer chains can be directly transformed into macroradicals under electron radiation, which was also applied to a covalent modification of CNTs [20].

On the other hand, to obtain well-dispersed CNTs/polymer composites, various fabrication methods have been developed, such as in situ polymerization [21], solution blending [22–24], melt blending [25–32], and solid-state mechanochemical pulverization [33]. More recently, it was

J. Zheng · Z. Zhu · J. Qi · Z. Zhou · P. Li · M. Peng (✉)
Department of Polymer Science & Engineering, Key Laboratory of Macromolecular Synthesis and Functionalization, Ministry of Education, Zhejiang University, Hangzhou 310027, People's Republic of China
e-mail: pengmao@zju.edu.cn

J. Zheng
State Key Laboratory of Polymer Physics and Chemistry, Changchun Institute of Applied Chemistry, Chinese Academy of Sciences, Changchun 130022, People's Republic of China

found that the combination of solid-state mechanochemical pulverization and melt-mixing could significantly improve the dispersion of CNTs in iPP and the properties of the final composites [34]. In situ macroradical addition during high shear melt blending was also successfully developed to fabricate SWNTs/PP composites using benzoyl peroxide (BPO) as an initiator [35]. BPO was heat decomposed into free radicals that attack iPP chains to generate macroradicals for the addition reaction. In situ polymerization of propylene on CNTs encapsulated by catalyst molecules was demonstrated to be effective in preparing CNTs/iPP composites with good distribution of CNTs [36, 37].

In this study, we report on a mild and effective method to prepare iPP-grafted MWNTs (iPP-g-MWNTs) by direct macroradical addition in a hot xylene solution of iPP, MWNTs, and BPO under sonication. Different from the previously reported methods for preparing CNTs/iPP composites, in this study, the iPP-g-MWNTs were successfully separated and purified by repeated hot vacuum filtration at about 130 °C to remove the ungrafted iPP and any other soluble by-products, so that the characterization of the chemical structure and quantitative determination of the grafting ratio of iPP-g-MWNTs became possible. At the same time, because MWNTs are less reactive than SWNTs in free radical addition, it is expected that the reaction in xylene under sonication possibly facilitates the graft reaction. Furthermore, to better understand the influence of surface grafting of MWNTs on the composite properties, iPP-g-MWNTs/iPP composites were prepared by conventional melt blending. The mechanical properties and crystallization behavior of the composites were investigated preliminarily and compared with those of neat iPP and the composites of pristine MWNTs filled iPP (MWNTs/iPP).

Experimental

Materials

MWNTs were supplied by Shenzhen Nano-Technologies Port Co. Ltd., China, with a purity of above 95%, diameter of 10–20 nm and length 5–15 μm. iPP (T300, MFI = 3 g/10 min, $M_w = 3.3 \times 10^5$, $M_n = 8.1 \times 10^4$) was purchased from Sinopec Shanghai Petrochemical Co., Ltd., China. Xylene and BPO were of analytical grades. All chemicals and materials were used as received.

Preparation of iPP-g-MWNTs and the control sample

0.4 g of MWNTs and 1.0 g of iPP were mixed in 100 mL of xylene and magnetically stirred at about 140 °C until iPP was dissolved completely. The suspension was cooled to about 85 °C, at which iPP remained soluble in xylene. Then, 1.0 g of BPO was added as the initiator of the free-radical grafting reaction. The suspension was sonicated for 2 h in a bath sonicator (EQ-50E, 50W, 40 kHz, Kunshan Shumei Ultrasonic Instrument Co., Ltd., China) at about 85 °C. After reaction, the suspension was heated to 130 °C and iPP-g-MWNTs were separated by hot vacuum filtration through poly(vinylidene fluoride) microfiltration membranes with an average pore size of 0.45 μm. In the home-made hot vacuum filtration system, the temperature of the suspensions was maintained at 130 °C, so that the ungrafted iPP did not crystallize or precipitate and was filtrated through the microfiltration membranes. The separated iPP-g-MWNTs were redispersed in hot xylene and vacuum filtrated at 130 °C for 5 times to remove the ungrafted iPP. The products were dried in a circular oven at 80 °C overnight. To exclude the possibility that the ungrafted iPP in xylene were physically adsorbed on iPP-g-MWNTs and not removed by hot vacuum filtration, a control sample (c-MWNTs) was prepared, in which MWNTs was simply dispersed in a xylene solution of iPP, mechanically stirred at 85 °C for 2 h, and then vacuum filtrated and washed under the same conditions for iPP-g-MWNTs. BPO-grafted MWNTs (BPO-g-MWNTs) was also prepared by the same method for the preparation of iPP-g-MWNTs in the absence of iPP.

To analyze the mechanism of the grafting reaction, the ungrafted iPP and by-products of the grafting reaction were collected by drying the filtrate. Besides ungrafted iPP, a sublimatable by-product that was soluble in polar solvents such as ethanol and dimethyl ether and formed crystals after cooling was found and observed by FTIR. The ungrafted iPP was washed and dried for high-temperature gel permeation chromatography (GPC) measurement.

Preparation of MWNTs/iPP and iPP-g-MWNTs/iPP composites

iPP-g-MWNTs were blended with iPP by melt mixing in a Haake rheocord 90 torque rheometer (Germany) at 180 °C for 20 min at a rotating rate of 50 rpm to obtain the iPP-g-MWNTs/iPP composites. The MWNTs/iPP composites were prepared in the same method using pristine MWNTs instead. The composites were hot-pressed into sheets with a thickness of 1 mm at 180 °C, and cut into dumbbell specimens with a length of 25 mm, a width of 4 mm and a thickness of 1 mm for the tensile tests.

Characterizations

Structure of iPP-g-MWNTs

The chemical structure of iPP-g-MWNTs was characterized by FTIR using KBr pellets on an FTIR spectrometer (Vector-22, Bruker, Germany). Raman spectra were recorded by a

dispersive Raman spectrometer (Nicolet Almega Thermo, USA). TG analysis was performed on a Pyris 1 thermal gravimetric analyzer (Perkin-Elmer, USA) under nitrogen atmosphere. The samples were heated to 100 °C from room temperature, maintained for 10 min, and then heated to 800 °C at a rate of 20 °C/min. High-temperature GPC was utilized to evaluate the molecular weight (MW) of ungrafted PP, in which the mobile phase was 1,2,4-trichlorobenzene (TCB) at a temperature of 150 °C and a flow rate of 1 mL/min. The samples were prepared at a concentration of about 0.5 wt% in TCB solutions. MWs were determined using a universal calibration curve with polystyrene standards. The morphologies of iPP-g-MWNTs were observed by transmission electron microscopy (TEM, JEM 1230, JEOL, JP) operated at 120 kV.

Mechanical properties and morphology of the composites

The tensile tests were carried out at ambient conditions on a CMT-2000 electromechanical universal testing machine (SANS, Shenzhen, China). The crosshead speed was kept constant at 2 mm/min for all the specimens. The morphology of the dumbbell specimens after the tensile test was observed by field emission scanning electron microscopy (FE-SEM, SIRION-100, FEI, The Netherlands). Some specimens were torn along the extensional direction after the tensile experiments to observe the morphology of the CNTs exposed on the side surfaces of the torn pieces.

Crystallization behavior of the composites

The isothermal crystallization behavior of neat iPP, iPP-g-MWNTs/iPP, and MWNTs/iPP composites were studied with differential scanning calorimetry (DSC). A Perkin-Elmer Pyris 1 DSC apparatus (USA) with nitrogen purge was used. The samples were heated to 200 °C and isothermally treated for 5 min to eliminate any thermal history, then, rapidly cooled to the isothermal crystallization temperatures (T_c) and maintained for a certain time until crystallization was completed. The spherulite morphologies were observed using a XPT-7 polarized optical microscope (POM) (Jiangnan Optics and Electronics Co., Ltd., Nanjing, China). The samples were sandwiched between two microscope glass slides, melted at 180 °C for 10 min, hot-pressed and cooled down to 130 °C and hold for about 2 h. The thickness of the sample films was about 100 μm.

Results and discussion

TG curves

TG was used to determine whether iPP could be grafted onto the surface of MWNTs, and whether repeated hot vacuum filtration and redispersion in xylene could remove the ungrafted iPP. As shown in the inset of Fig. 1a, c-MWNTs (curve 2) has a slightly larger weight loss (3.9 wt%) than pristine MWNTs (curve 1), and in the corresponding dTG curve (curve 2 in Fig. 1b), a small decomposition peak appears at around 475 °C, which is ascribed to the pyrolysis of iPP. This indicates that a small amount of iPP was still physically adsorbed on MWNTs, but fortunately, the amount of physically adsorbed iPP was very small, and most adsorbed iPP was removed by repeated hot vacuum filtration. As to the BPO-g-MWNTs (curve 3 in the inset of Fig. 1a), the weight loss is larger than that of pristine MWNTs by about 2.6 wt% and the corresponding dTG curve (curve 3 in Fig. 1b) shows a small pyrolysis peak at 256 °C, indicating that the free radicals generated by the decomposition of BPO can also be attached to the surface of MWNTs, but the grafting ratio is relatively small. The weight loss of iPP-g-MWNTs (curve 4 in the inset of Fig. 1a) is about 10.5 wt%, which is larger than that of pristine MWNTs and 8.0 wt% larger than that of MWNTs separated from the simple mixture of MWNTs and iPP in xylene. The corresponding dTG curve (curve 4 in Fig. 1b) exhibits a major pyrolysis peak at about 475 °C and a small pyrolysis peak at about 259 °C, respectively. It is noted that

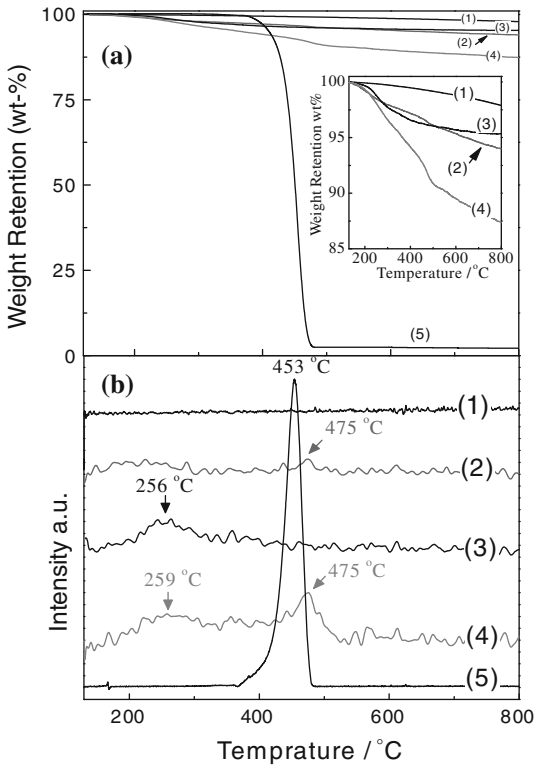

Fig. 1 **a** TG curves of pristine MWNTs (*1*), c-MWNTs (*2*), BPO-g-MWNTs (*3*), iPP-g-MWNTs prepared at a mass ratio of BPO/iPP/MWNTs = 0.4/1.0/0.4 g (*4*), and neat iPP (*5*); **b** the dTG curves corresponding to (**a**). The inset of (**a**) shows the details of the TG curves for the samples (*1*)–(*4*)

the temperature for the maximum weight loss of iPP-g-MWNTs is 22 °C higher than that of neat iPP (curve 5 in Fig. 1b), indicating that the heat resistance of grafted iPP is better than that of neat iPP, due to certain interactions between MWNTs and the grafted iPP. Similar effect was also observed in CNTs/PP composites prepared by in situ polymerization of propylene on CNTs [37]. Therefore, we conclude that the iPP macroradicals initiated by BPO in xylene can be grafted onto the surface of MWNTs. The residual weight of neat iPP is about 2.1 wt%, accordingly, the grafting ratio (i.e., ratio of grafted polymer to nanotube product) of iPP-g-MWNTs can be calculated to be about 9.1 wt%.

Raman and FTIR spectra

In Raman spectra of CNTs, the disorder mode (D band ~ 1336 cm^{-1}) is indicative of the presence of sidewall defects on CNTs arising from the sp3 C–C bonds. The tangential mode (G band ~ 1578 cm^{-1}) is due to the sp2 C=C bond stretching vibrations. The ratios of the G to D integrated peak reflect the change in the structure of CNTs caused by sidewall functionalizations. Larger D/G ratio illustrates more sp3 defects on CNTs. Figure 2 shows the Raman spectra of pristine MWNTs and the modified MWNTs with different BPO/iPP mass ratios during modification. The D/G ratios are shown in the inset of Fig. 2, which show that the D/G ratios of iPP-g-MWNTs are higher than that of pristine MWNTs, confirming the grafting of iPP chains on the surface of MWNTs. In the absence of iPP (Fig. 2b), grafting reaction of BPO also occurs, but the D/G ratio is somewhat lower than those of iPP-g-MWNTs.

The FTIR spectra of pristine MWNTs, iPP-g-MWNTs, and neat iPP are shown in Fig. 3. As aforementioned, TG

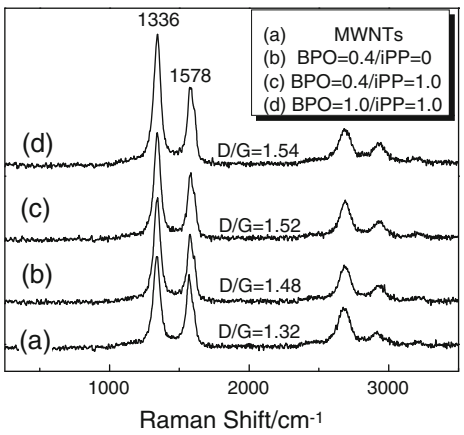

Fig. 2 Raman spectra and the D/G values of (*a*) pristine MWNTs, (*b*) MWNTs reacted with BPO, and iPP-g-MWNTs prepared at the BPO/iPP mass ratio of (*c*) 0.4/1.0 and (*d*) 1.0/1.0, respectively

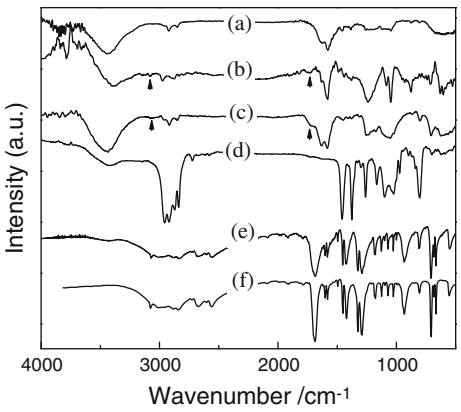

Fig. 3 IR spectra of (*a*) pristine MWNTs, (*b*) BPO-MWNTs, (*c*) iPP-g-MWNTs, (*d*) neat iPP, (*e*) the sublimatable by-product separated from the filtrate, and (*f*) benzoic acid. The iPP-g-MWNTs was prepared at the mass ratio of BPO/iPP/MWNTs = 0.4/1.0/0.4 g

analysis indicates that ungrafted and physically adsorbed iPP can be mostly removed by repeated hot vacuum filtration, therefore, the adsorption bands at around 2980 cm^{-1} in the FTIR spectrum of iPP-g-MWNTs can be assigned to the saturated C–H stretching of the grafted iPP chains and the adsorption bands at 1460 and 1380 cm^{-1} can be ascribed to the bending vibration of methyl groups ($–CH_3$) in iPP, demonstrating that iPP has been successfully grafted onto the surface of MWNTs. Furthermore, the bands at about 1730 cm^{-1} (C=O, ester) and 3050 cm^{-1} (aromatic CH stretching) for the BPO-g-MWNTs and iPP-g-MWNTs indicate that the small-molecular benzoic acid free radicals generated by the decomposition of BPO can also be grafted onto the sidewall of MWNTs.

In studying the in situ macroradical addition of iPP on SWNTs by melt blending, McIntosh et al. [35] proposed that the initiator BPO was heat decomposed into benzyl free radicals attacking the hydrogen atoms of iPP, which directly generated macroradicals or initiated the β-scission of iPP chains to produce macroradicals for the addition reaction. As mentioned above, the TG results show that there exist a small decomposition peak at around 259 °C and a large decomposition peak at around 475 °C for iPP-g-MWNTs, indicating that both small molecular weight free radicals and macromolecular free radicals are responsible for the addition reactions in this study. The results of high-temperature GPC show that the molecular weight of the ungrafted iPP (separated from the filtrate) is decreased by about 25%, due to the degradation of iPP macromolecules caused by the attack of free radicals and sonication during the grafting reaction. Furthermore, FTIR demonstrates that the sublimatable by-product separated from the filtrate is benzoic acid (Fig. 4e), revealing that the benzoic acid free radicals also play an important role in the preparation of iPP-g-MWNTs. This phenomenon has not

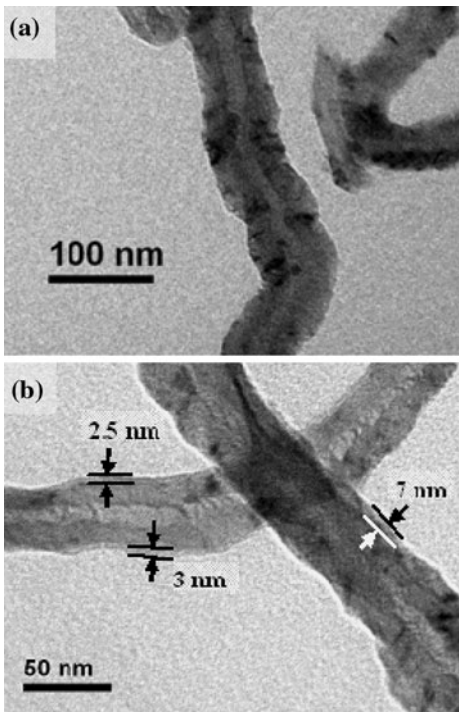

Fig. 4 TEM images of **a** c-MWNTs and **b** iPP-g-MWNTs

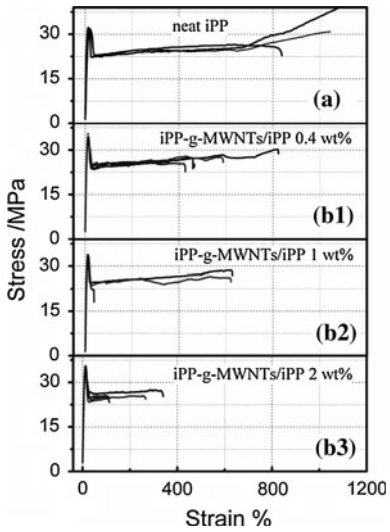

Fig. 5 Stress-strain curves of **a** neat iPP, and iPP-g-MWNTs/iPP composites with filler contents of **b1** 0.4 wt%, **b2** 1.0 wt%, and **b3** 2.0 wt%

been reported previously. It should be mentioned that the amount of BPO used in this study was high, and the grafting reaction was conducted at 85 °C in xylene, while the in situ functionalization by melt-mixing was conducted at high temperatures up to 175 °C [35]. Further investigation is necessary to completely illuminate the mechanism of the grafting reaction.

TEM observation

Figure 4 presents the TEM images of c-MWNT and iPP-g-MWNTs sufficiently purified by hot vacuum filtration. The surface of the control MWNT sample (Fig. 4a) is relatively clean, indicating that most iPP physically adsorbed on the surface of MWNTs can be removed by sufficient hot vacuum filtration, which is consistent with the result of TG. On the contrary, iPP-g-MWNTs obviously have a thin layer of polymer on the surface, as shown in Fig. 4b. The thickness of the iPP layer on the surface of MWNTs ranges from 2.5 to 7.0 nm and the MWNTs were almost completely encapsulated by the polymer layer.

Mechanical properties

As shown in Fig. 5, the stress–strain curve of neat iPP exhibits a sharp yield and then stretching to a very large elongation at break of about 1000% with an obvious strain hardening (cold drawing) behavior. The stress–strain curves of the iPP-g-MWNTs/iPP composites (Fig. 5) also exhibit yield points and cold drawing regions, while in comparison with neat iPP, the elongations at break decrease gradually with the increase of filler content. Neat iPP exhibits a continuous increasing of tensile strength after yielding due to the orientation of macromolecules under stress. Differently, the iPP-g-MWNTs/iPP composites display a characteristic wave-like pattern in the cold drawing region and a gradual increase of strength. This process is similar to the sequential breakage of crosslinked parts of crosslinked SWNTs/polyelectrolyte hybrid membranes prepared by layer-by-layer assembly [38], and that of coiled molecules observed in natural composites, such as seashells and bones [39, 40]. Therefore, it is reasonable to say that the reorganization of the microstructure of the composite under stress is likely to be responsible for the wave-like pattern and the increase of the slope of the stretching curve. However, tensile hardening at high strain is not observed, indicating that existence of iPP-g-MWNTs prevents the sufficient stretching and orientation of iPP macromolecules.

On the contrary, for the MWNTs/iPP composites, the elongations at break are very low and no plateau region (cold drawing region) corresponding to plastic deformations is observable on the stress–strain curves, even when the content of MWNTs is as low as 0.4 wt% (Fig. 6). It is interesting that at low filler contents of MWNTs (0.4 and 1 wt%), the stress of some MWNTs/iPP specimens decreases step by step after the yield point (Fig. 6). It was observed the dumb-bell specimens became ripped or torn along the longitudinal axis during the tensile test. The ripped pieces broke one by one, so that step-by-step decreases in the stress–strain curves were observed.

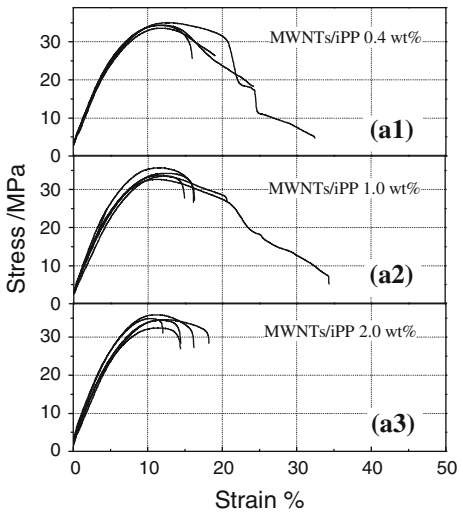

Fig. 6 Stress–strain curves of MWNTs/iPP composites with pristine MWNT contents of **a1** 0.4 wt%, **a2** 1.0 wt%, and **a3** 2.0 wt%

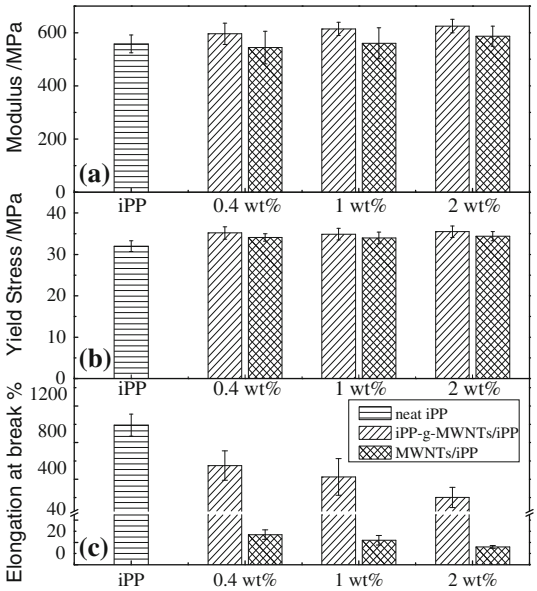

Fig. 7 Comparison of the mechanical properties of neat iPP, iPP-g-MWNTs/iPP, and MWNTs/iPP composites: **a** Young's modulus, **b** yield stress, and **c** elongation at break

Figure 7 shows that the average yield stress and Young's modulus of both iPP-g-MWNTs/iPP and MWNTs/iPP composites are higher than those of neat iPP. At the same time, the yield stress and Young's modulus of iPP-g-MWNTs/iPP are somewhat larger than those of MWNTs/iPP composites, indicating that iPP-g-MWNTs increases the mechanical properties of iPP more effectively than pristine MWNTs. The data errors for the MWNTs/iPP composites are somewhat larger than those of iPP-g-MWNTs/iPP composites, indicating that the structure of the latter is more uniform than that of the former.

The improved mechanical properties of the iPP-g-MWNTs/iPP composites can be owed to the better dispersion of iPP-g-MWNTs in iPP. The grafted iPP chains on MWNTs increase the interactions between MWNTs and iPP, so that stress can be transmitted between interfaces. On the contrary, the agglomeration and entanglement of pristine MWNTs in iPP bring about poor dispersion and the formation of large filler aggregates [26]. As a result, stress concentration and crack propagation centering around the large MWNT aggregates occur during tensile tests, leading to a brittle fracture [2, 41]. Moreover, the elongations at break of iPP-g-MWNTs/iPP are much larger than those of MWNTs/iPP, which has been seldom mentioned previously in the literature. This shows that the immobilized iPP chains on iPP-g-MWNTs are more effective than small-molecular compounds used to modify CNTs in increasing the interface bonding [42, 43].

Morphology

Figure 8a1 shows the morphology of a iPP-g-MWNTs/iPP specimen (0.4 wt%) after being tensile fractured. A fibrous fractured surface with highly stretched regions is observed due to the large elongation at break of iPP-g-MWNTs/iPP at high strain, indicating the occurrence of a ductile fracture. Figure 8a2 shows the typical morphology of the side surface of a piece of iPP-g-MWNTs/iPP specimen which was torn off along the stretching direction (indicated by the arrow) during the tensile test. The nanotubes align along the stretching direction, indicating the occurrence of orientation of iPP-g-MWNTs under the tensile stress, which contributes to the enhanced yield strength and modulus of the composites. In contrast, the tensile-fracture surface of MWNTs/iPP composites (0.4 wt%) shows the existence of large MWNT agglomerates (Fig. 8b1) and no fibrous morphology was observed.

At a higher filler content of 2 wt%, aggregates of CNTs can be observed on the tensile-fracture surfaces of both the iPP-g-MWNTs/iPP (Fig. 8a3) and MWNTs/iPP composites (Fig. 8b2, b3). But there are obvious differences between the two composites. The iPP-g-MWNT aggregates are tightly wrapped by iPP, indicating that the interaction between the iPP-g-MWNT aggregates and the iPP matrix is strong. On the contrary, for the MWNTs/iPP composites, the MWNT aggregates are completely pulled out of the iPP matrix, forming nodules or caves on the fractured surface (as indicated by the arrows in Fig. 8b2). The zoom-in FE-SEM image in Fig. 8b3 shows that there exists an obvious crack between the MWNT aggregate and the iPP matrix, revealing the poor interphase adhesion. This explains the brittle fracture and low elongations at break of the MWNTs/iPP composites. Furthermore, the zoom-in FE-SEM image in Fig. 8a4 shows that iPP-g-MWNTs in

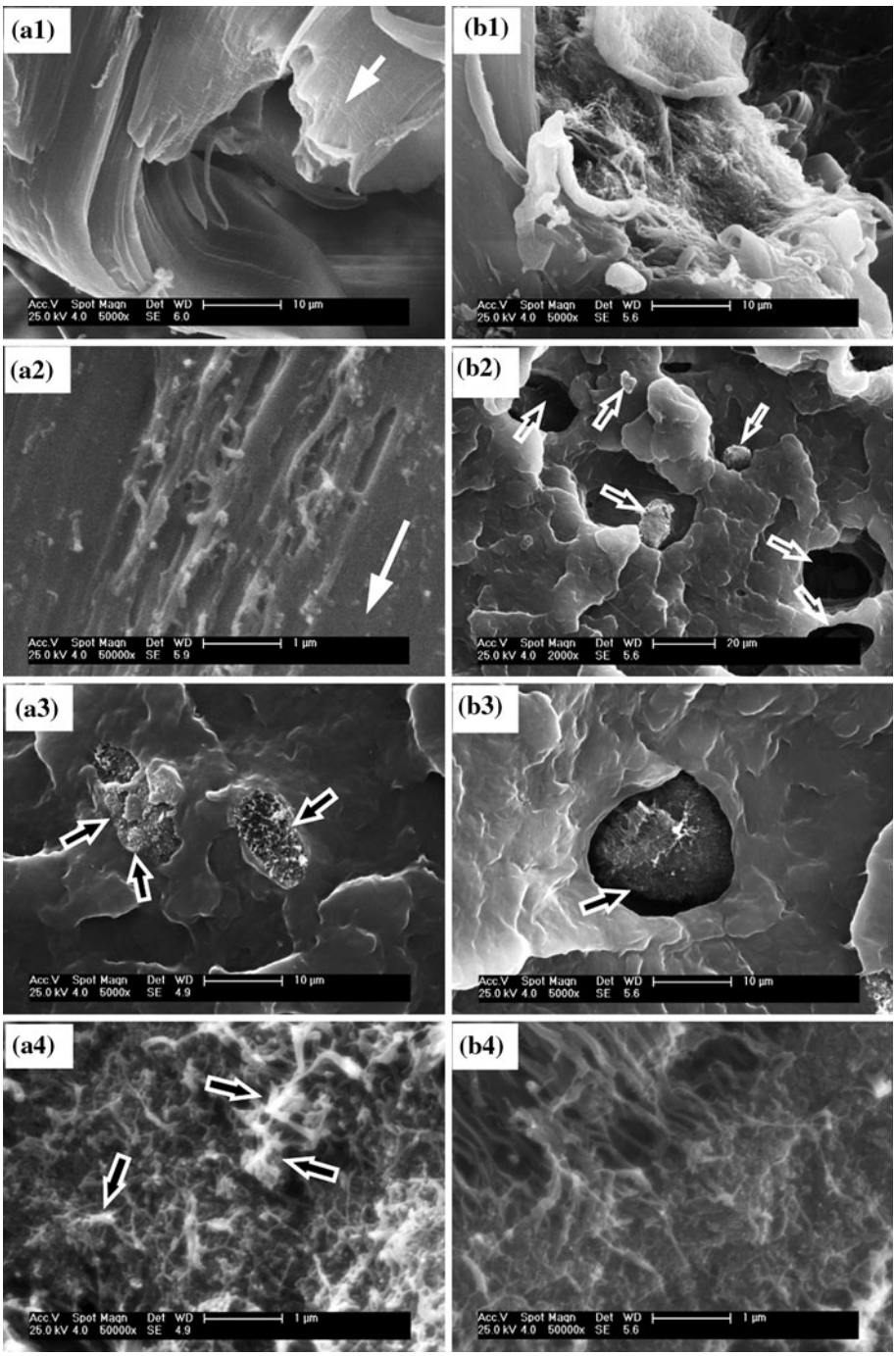

Fig. 8 FE-SEM images of the tensile-fracture end (**a1**) and the side surface (**a2**) of a torn piece of a iPP-g-MWNTs/iPP composite (0.4 wt%), the tensile-fracture surface of a iPP-g-MWNTs/iPP composite (2 wt%) (**a3**), the iPP-g-MWNT agglomerates (**a4**), the tensile-fracture surface of a MWNTs/iPP composite of 0.4 wt% (**b1**) and 2 wt% (**b2**, **b3**), and the MWNT agglomerates (**b4**)

their aggregates are rough for being wrapped or adhered by iPP, and some of them stand upwardly under the effect of tensile stress. In contrast, pristine MWNTs in their aggregates (Fig. 8b4) are relatively smooth and clean, due to the weak interactions between MWNTs and iPP.

Spherulite morphology and crystallization behavior

The spherulite morphology of the iPP-g-MWNTs/iPP composites were observed and compared with those of MWNTs/iPP. The spherulites of neat iPP are larger than 100 μm (Fig. 9a). However, POM images in Fig. 9 show that the spherulites of MWNTs/iPP and iPP-g-MWNTs/iPP composites formed under the same crystallization conditions for neat iPP are irregularly shaped with a much smaller size, and no spherulites with distinguishable Maltese-cross are observable (Fig. 9b, c). This indicates that both MWNTs and iPP-g-MWNTs have a strong nucleation effect on the crystallization of iPP [44]. Furthermore, pristine MWNTs are difficult to disperse uniformly in iPP

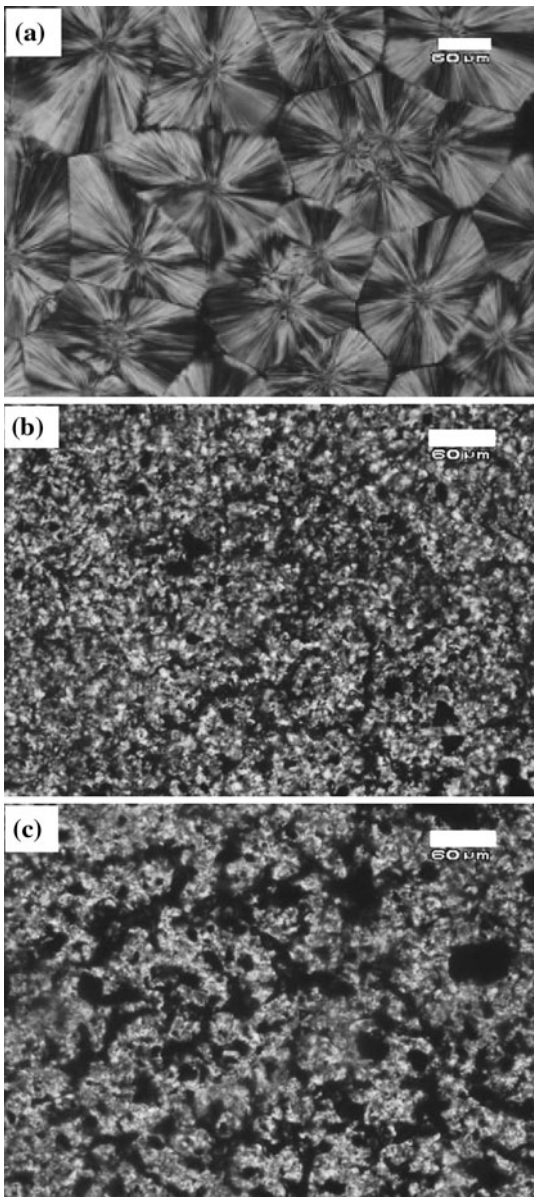

Fig. 9 POM images of (**a**) pure iPP, (**b**) iPP-g-MWNTs/iPP (2.0 wt%), and (**c**) MWNTs/iPP (2.0 wt%) composites. The length of the scale bars is 60 μm

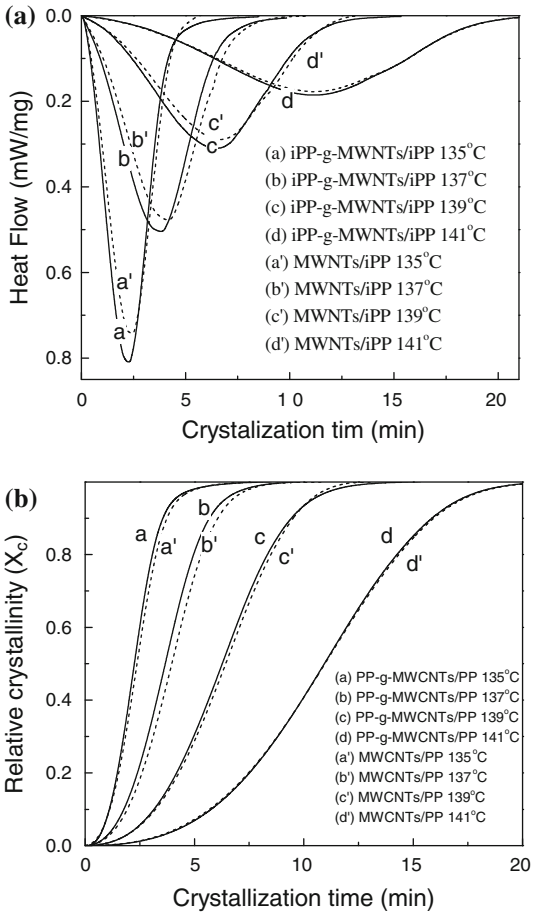

Fig. 10 **a** Heat flow curves of isothermal crystallization, and **b** the dependence of relative crystallinity on the crystallization time for the iPP-g-MWNTs/iPP (2.0 wt%) and MWNTs/iPP (2.0 wt%) composites

Table 1 Crystallinity of neat iPP, iPP-g-MWNTs/iPP (2.0 wt%), and MWNTs/iPP (2.0 wt%) composites at various isothermal crystallization temperatures

Temperature (°C)	Crystallinity (%)		
	iPP	iPP-g-MWNTs/iPP	MWNTs/iPP
135	56.2	53.3	51.7
137	57.1	54.8	54.8
139	56.8	55.9	55.3
141	58.2	56.1	53.3

and large agglomerates are observed. Both the amount and the size of the agglomerates increase with the increase of the MWNT content. Some MWNT agglomerates are of several tens of micrometers in size. On the contrary, the dispersion of iPP-g-MWNTs in iPP is significantly improved. Although agglomerates can still be observed, the size is much smaller and the distribution is more uniform.

The isothermal crystallization behavior was investigated by DSC. Figure 10a presents the heat flow of MWNTs/iPP and iPP-g-MWNTs/iPP composites with a filler content of 2 wt% at different temperatures. Crystallinities (X_c) were calculated from exothermic enthalpy (ΔH_c) of the heat flow curves using $X_c = \Delta H_c/[(1 - \phi) \cdot \Delta H_m)]$, where ΔH_m is the heat fusion of iPP with 100% crystallinity (209 J/g) [37] and ϕ is mass fraction of CNTs, as shown in Table 1. The crystallinities of iPP-g-MWNTs/iPP and MWNTs/iPP composites are slightly lower than that of neat iPP. It is thought that CNTs may limit the mobility and diffusion of macromolecular chains and thereby bring about defects to iPP crystallites. Previous studies have shown that the

influence of CNTs on the crystallinity of iPP is rather complicated. Both decrease [43] and increase in the crystallinity of polypropylene [45, 46] induced by CNTs has been reported. Some other studies did not show definite correlations between crystallinities and CNTs content [22, 37, 47]. This may result from the differences in the materials and the methods for preparing composites used by different authors and the differences in the dispersion state of CNTs in iPP and the conditions for crystallization.

The relative degree of crystallinity during isothermal crystallization (X_t) is defined as the ratio of heat generated at time t against the entire heat generated during crystallization, as given by the following equation:

$$X_t = \int_0^t (\mathrm{d}H/\mathrm{d}t)\,\mathrm{d}t \Big/ \int_0^\infty (\mathrm{d}H/\mathrm{d}t)\,\mathrm{d}t \qquad (1)$$

where $\mathrm{d}H/\mathrm{d}t$ is the rate of heat evolution. The relationship of X_t with time was curved in Fig. 10b. It is noted that the crystallization rate of iPP-g-MWNTs/iPP composites is somewhat faster than that of MWNTs/iPP composites. The isothermal crystallization was analyzed on the basis of the Avrami equation: $X_t = 1 - \exp(-kt^n)$ or rewritten as $\log[-\ln(1 - X_t)] = \log k + n\log t$, where n is the Avrami exponent, a parameter dealing with the nucleation mechanism and crystal growth geometry, k is the crystallization rate coefficient, as shown in Fig. 11.

The primary crystallization of neat iPP follows the linear Avrami equation (Fig. 11A) and the slopes of Avrami plots remain unchanged until the late stage of crystallization when the spherulites impingement happens, giving a single exponent, n_1. The Avrami exponents of neat iPP are between 2.5 and 3, indicating an ordinary thermal nucleation process followed by a three-dimensional crystal growth. As to the effect of the incorporation of CNTs on the Avrami exponents, there are controversial discussions in the literature [44–49]. Our results suggest that the Avrami exponents of CNTs-containing composites depend on both temperature and the conversion of crystallinity. From Fig. 11B and C, it can be found that the slopes of the Avrami plots for the iPP-g-MWNTs/iPP and MWNTs/iPP composites tend to increase during crystallization. Therefore, we suggest that our samples do not have a single Avrami exponent but multiple exponents changing from n_0 to n_1 with the increase of relative crystallinity X_t. Also, with the increase of T_c, the phenomenon is more obvious. At relatively low conversion of crystallization ($X_t < 20\%$, or $\log[-\ln(1 - X_c)] < -0.65$), the Avrami exponents are somewhat lower than those of neat iPP, which can be ascribed to a reduction in the dimensionality of the growth process at the early stage of crystallization, due to the heterogeneous nucleation on the cylindrical nanofiber surfaces [44]. This is in good agreement with the previous reports, which shows that both SWNTs and MWNTs have strong nucleation effect on the crystallization behavior of iPP, which brings about a increased crystallization speed at low filler contents [34, 37, 40, 45, 49]. Furthermore, exponents of iPP-g-MWNTs/iPP are slightly lower than those of MWNTs/iPP, indicating that the nucleation effect of iPP-g-MWNTs is stronger than MWNTs. With the increase of temperature and relative crystallinity X_t, the Avrami exponents of the composites increase and become larger than those of neat iPP. This is in agreement with the report of Kaminsky et al. [36] who found that the Avrami exponents increased with the increase of temperature and filler content of CNTs.

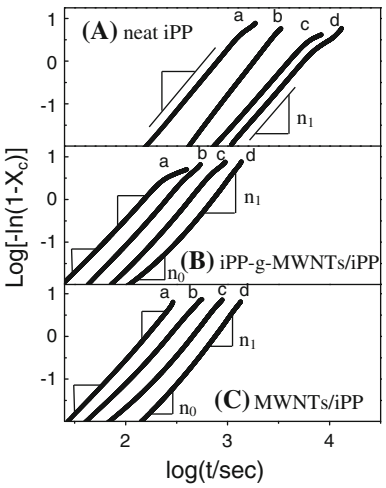

Fig. 11 Avrami plots of **A** neat iPP, **B** the iPP-g-MWNTs/iPP (2.0 wt%), and **C** MWNTs/iPP (2.0 wt%) composites isothermally crystallized at (*a*) 135 °C, (*b*) 137 °C, (*c*)139 °C, and (*d*) 141 °C

The crystallization half times ($t_{1/2}$) were calculated as $t_{1/2} = (\ln 2/k)^{1/n}$, in which the n_1 values were used as the Avrami exponents for the composites. The crystallization half times were also obtained directly from the $X_t \sim t$ curves in Fig. 10b, denoted as $T_{1/2}$. The Avrami exponents, $\log k$, $t_{1/2}$ and $T_{1/2}$ values are summarized in Table 2.

As to the $\log k$ values, at any temperature, the $\log k$ values of iPP-g-MWNTs/iPP and MWNTs/iPP composites are much higher than those of neat iPP. The $\log k$ values of iPP-g-MWNTs/iPP are slightly higher than those of MWNTs/iPP, revealing that the crystallization rate of iPP-g-MWNTs/iPP is faster than that of MWNTs/iPP, in good agreement with the result obtained from $t_{1/2}$.

The relatively faster crystallization rate of iPP-g-MWNTs/iPP composites should be related to the grafted iPP chains on the surface of MWNTs and the better dispersion of iPP-g-MWNTs in the iPP matrix. Because of the relatively smaller size and more uniform distribution of the MWNT agglomerates in iPP, the larger interface area favors the heterogeneous nucleation and accelerates the crystallization of iPP.

Table 2 Avrami exponents, log k, $t_{1/2}$, and $T_{1/2}$ values of neat iPP, iPP-g-MWNTs/iPP (2.0 wt%) and MWNTs/iPP (2.0 wt%) composites at various isothermal crystallization temperatures

Samples	Temperature (°C)	Log k	n_0	n_1	$t_{1/2}$ (s)	$T_{1/2}$ (s)
iPP	135	−8.29	/	2.86	697	701
	137	−9.18	/	2.84	1501	1504
	139	−9.26	/	2.73	3165	3174
	141	−9.73	/	2.76	4356	4376
iPP-g-MWNTs/iPP	135	−5.65	2.43	2.59	132	135
	137	−6.69	2.16	2.78	224	220
	139	−7.54	2.40	2.87	373	376
	141	−8.75	2.23	3.06	642	656
MWNTs/iPP	135	−6.28	2.50	2.85	141	142
	137	−6.84	2.30	2.82	234	238
	139	−8.01	2.37	3.04	383	385
	141	−9.09	2.35	3.15	685	658

Conclusion

iPP-g-MWNTs were synthesized by macroradical addition in the xylene solution under mild conditions and successfully purified by repeated hot vacuum filtration and redispersion in hot xylene to remove the ungrafted iPP. Both small-molecular benzoic acid free radicals and iPP macromolecular radicals were grafted onto the surface of MWNTs. The yield strength, Young's modulus especially the elongations at break of the iPP-g-MWNTs/iPP composites are higher than those of MWNTs/iPP composites, because of the improved dispersion of iPP-g-MWNTs and the interfacial interactions. Previous studies showed that the temperatures and time for melt blending and the rotating speed of the rotors play crucial roles in determining the dispersion state of CNTs [34], therefore, further studies should be conducted to optimize the conditions for melt blending to improve the dispersion of iPP-g-MWNTs in iPP.

Acknowledgement We appreciate financial support from the National Natural Science Foundation of China (20574060 and 50773066).

References

1. Ajayan PM, Stephan O, Colliex C, Trauth D (1994) Science 265:1212
2. Moniruzzaman M, Winey KI (2006) Macromolecules 39:5194
3. Finegan IC, Tibbetts GG, Glasgow DG, Ting JM, Lake ML (2003) J Mater Sci 38:3485. doi:10.1023/A:1025109103511
4. Wang K, Zhou CJ, Tang CY, Zhang Q, Du RN, Fu Q, Li L (2009) Polymer 50:696
5. Kovalchuk AA, Shevchenko VG, Shchegolikhin AN, Nedorezova PM, Klyamkina AN, Aladyshev AM (2008) J Mater Sci 43:7132. doi:10.1007/s10853-008-3029-8
6. Ning NY, Luo F, Wang K, Du RN, Zhang Q, Chen F, Fu Q (2009) Polymer 50:3851
7. Sengupta R, Ganguly A, Sabharwal S, Chaki TK, Bhowmick AK (2007) J Mater Sci 42:923. doi:10.1007/s10853-006-0011-1
8. Rakhimkulov AD, Lomakin SM, Dubnikova IL, Shchegolikhin AN, Ya Davidov E, Kozlowski R (2010) J Mater Sci 45:633. doi:10.1007/s10853-009-3977-7
9. Banerjee S, Hemraj-Benny T, Wong SS (2005) Adv Mater 17:17
10. Liu P (2005) Eur Polym J 41:2693
11. Kitano H, Tachimoto K, Gemmei-Ide M, Tsubaki N (2006) Macromol Chem Phys 207:812
12. Ying YM, Saini RK, Liang F, Sadana AK, Billups WE (2003) Org Lett 5:1471
13. Park SJ, Cho MS, Lim ST, Choi HJ, Jhon MS (2003) Macromol Rapid Commun 24:1070
14. Sung JH, Kim HS, Jin HJ, Choi HJ, Chin IJ (2004) Macromolecules 37:9899
15. Liu YQ, Yao ZL, Adronov A (2005) Macromolecules 38:1172
16. Qin SH, Qin DQ, Ford WT, Resasco DE, Herrera JE (2004) Macromolecules 37:752
17. Guo G, Yang D, Wang C (2006) Macromolecules 39:9035
18. Liu YL, Chen WH (2007) Macromolecules 40:8881
19. Lou X, Detrembleur C, Pagnoulle C, Jérôme R, Bocharova V, Kiriy A, Stamm M (2004) Adv Mater 16:2123
20. Sullivan ME, Klosterman D, Palmese GR (2007) Nucl Instrum Methods Phys Res Sect B 265:352
21. Srivastava R, Banerjee S, Jehnichen D, Voit B, Böhme F (2009) Macromol Mater Eng 294:96
22. Kearns JC, Shambaugh RL (2002) J Appl Polym Sci 86:2079
23. Yang JW, Hu JH, Wang CC, Qin YJ, Guo ZX (2004) Macromol Mater Eng 289:828
24. Almasri A, Ounaies Z, Kim YS, Grunlan J (2008) Macromol Mater Eng 293:123
25. Bao SP, Tjong SC (2008) Mater Sci Eng A 485:508
26. Tong X, Chen Y, Cheng HM (2005) J Mater Sci Technol 21:686
27. Andrews R, Jacques D, Minot M, Rantell T (2002) Macromol Mater Eng 287:39
28. Li Z, Ying Z, Liu M, Cheng HM (2005) New Carbon Mater 20:108
29. Lin B, Sundararaj U, Pötschke P (2006) Macromol Mater Eng 291:227
30. Kumar S, Doshi H, Srinivasarao M, Park JO, Schiraldi DA (2002) Polymer 43:1701
31. Seo MK, Park SJ (2004) Macromol Mater Eng 289:368
32. Fritzsche J, Lorenz H, Klüppel M (2009) Macromol Mater Eng 294:551
33. Xia HS, Wang Q, Li KS, Hu GH (2004) J Appl Polym Sci 93:378
34. Masuda J, Torkelson JM (2008) Macromolecules 41:5974
35. McIntosh D, Khabashesku VN, Barrera EV (2007) J Phys Chem C 114:1592
36. Funck A, Kaminsky W (2007) Compos Sci Technol 67:906
37. Kovalchuk AA, Shchegolikhin AN, Shevchenko VG, Nedorezova PM, Klyamkina AN, Aladyshev AM (2008) Macromolecules 41:3149
38. Mamedov AA, Kotov NA, Prato M, Guldi DM, Wicksted JP, Hirsch A (2002) Nat Mater 1:257
39. Thompson JB, Kindt JH, Drake B, Hansma HG, Morse DE, Hansma PK (2001) Nature 414:773
40. Smith BL, Schaffer TE, Viani M, Thompson JB, Frederick NA, Kindt J, Belcher A, Stucky GD, Morse DE, Hansma PK (1999) Nature 399:761
41. Seo MK, Lee JR, Park SJ (2005) Mater Sci Eng A 404:79
42. Assouline E, Lustiger A, Barber AH, Cooper CA, Klein E, Wachtel E, Wagner HD (2003) J Polym Sci B 41:520
43. Hou ZC, Wang K, Zhao P, Zhang Q, Yang CY, Chen DQ, Du RN, Fu Q (2008) Polymer 49:3582

44. Lee GW, Jagannathan S, Chae HG, Minus ML, Kumar S (2008) Polymer 49:1831
45. Grady BP, Pompeo F, Shambaugh RL, Resasco DE (2002) J Phys Chem B 106:5852
46. Rahmatpour A, Aalaie J (2008) J Macromol Sci Phys 47:929
47. Sandler J, Broza G, Nolte M, Schulte K, Lam YM, Shaffer MSP (2003) J Macromol Sci Phys B 42:479
48. Xu DH, Wang ZG (2008) Polymer 49:330
49. Chen JH, Yao BX, Su WB, Yang YB (2007) Polymer 48:1756